How Digital Fault Recorder Calibration Affects Fault Location

Ethan M. Mueller[1], Robert M. Orndorff[1], Micah J. Till[2]
[1]System Protection Automation & Analysis, [2]System Protection Engineering
Dominion Energy Virginia
ethan.m.mueller@dominionenergy.com

Amir Makki[3], Maria Rothweiler[4]
[3]Electrical Engineer, [4]Software Engineer
Philadelphia PA, United States

***Abstract*—Digital fault recorder (DFR) data can be used in megawatt/megavar calculations, frequency calculations, fault location, power quality studies, and more. All of these analyses are affected by factors that are not typically considered, such as potential transformer/current transformer ratios, the phase angle error, and magnitude calibration. For this study, we sampled DFR data for fault location calculations. The idea for this paper came about when a field technician asked about the real-world impact of calibrating a fault recorder and how calibration affects fault location accuracy. To study this problem, we first performed a series of fault location calculations using actual fault records, then introduced intentional variations meant to simulate calibration errors, and observe any differences. Our study results can be used to provide guidance for DFR maintenance policies regarding field calibration.**

***Keywords*—Digital fault recorder (DFR), magnitude, calibration**

I. Background

Dominion Energy has a fleet of over 250 Digital Fault Recorders (DFRs). These recorders are on a four-year maintenance cycle, and part of the maintenance involves calibrating the analog inputs. This is done by injecting a known quantity of voltage or current and verifying that the DFR reads the correct values. The test equipment providing the voltage or current is on a calibration program, so we have a reasonable expectation that any test will be accurate. Our calibration procedures specify an expected tolerance, which raised the question: What is the practical impact of calibration, and how tight do the tolerances really need to be? We thought that if we could get significant data on the impact of calibration, then we could fine-tune our procedures to ensure that we are getting "good enough" data from our recorders.

II. Methods

We selected 32 real-world faults as case studies for this paper. We ran the faults through an automated script that varies each input value by a specified amount. Using the adjusted values, the script then calculates fault location. In addition to varying voltage and current magnitude, we also varied phase angle and impedance to providedata for future studies.

Our calibration procedure calls for no greater than ± 0.5% calibration error. Voltages are calibrated at 100 V and currents at 5 A. This allows for a variation of ±0.5 volts and ±0.25 amps.

For the sample faults, we decided to change the input values by ±10%. Initially, we considered basing our percentage change on some nominal value, such as 67 V or 120 V secondary, but in the end what we really cared about was the percentage change in whatever value the recorder is measuring. This of course assumed that the DFR's measurement response is linear. We don't normally test for linearity when calibrating, but have done so in the past and noted no problems.

A problem arose with using ±10% change in input value when we measured the phase angle. Changing a 5° phase angle by 10% yields a far different result that changing a 120° angle by 10%. Therefore, we chose to simply vary phase angles by ±10°.

We decided to change the line parameters as well, to take advantage of automation, which makes tedious tasks much less tedious. While line parameters are not subject to calibration like analog inputs are, line characteristics do affect fault location. Variations of line parameters can illustrate errors in inaccurate line impedence studies.

When changing the line parameters, the line impedance is varied in polar and rectangular form. Changing individual impedance values in rectangular form allows us to see the effect of changing only resistance or reactance. Changing the values in polar form allows us to see the effects of changing the line angle. Detailed results of these variations will be covered in future work.

The simulated calibration results were recorded as a text (*.csv*) file and graphed. The file compiled each sample fault's variation matrices and fault location calculations. The variation matrix, or simulated calibration, was produced by varying the input values in a fault sample. For example, let's say a fault has three voltages—A, B, and C-phases; the goal is to vary the voltage from ±2% magnitude in 1% increments. For simplicity, let's also say that the voltage magnitudes are all 100 V. Three input values are taken at the time of a fault. When the phase voltage is varied by ±2%, the results yield 5 inputs ranging from 98 V to 102 V. For the first calibration state, the A-phase voltage is set to 98 V, while B and C-phase voltages are still 100V. This procedure is repeated for every input. So in our example of three inputs for one fault, varied over a 4% range, our study produced 15 different states of calibration. Table I

illustrates the outputs of this example. The states that were changed are marked in bold.

Table I
Example Variation Matrix

A Phase	B Phase	C Phase	Calibration State
98	100	100	1
99	100	100	2
100	100	100	3
101	100	100	4
102	100	100	5
100	**98**	100	6
100	**99**	100	7
100	**100**	100	8
100	**101**	100	9
100	**102**	100	10
100	100	**98**	11
100	100	**99**	12
100	100	**100**	13
100	100	**101**	14
100	100	**102**	15

In the example we used three inputs, but for our actual data we extracted 19 input values that were varied ±10% or ±10° in 0.5% increments, making a grand total of 779 different calibration states.

We then calculated the fault location for each state in two ways: using the simple impedance equations and the reactance method from IEEE C37.114 [2].

We used the simple impedance equations with the complex form of the input data to calculate measured fault impedance. We then divided the measured impedance by the line impedance to produce a fault location's magnitude value and angular value. We have learned through experience that this angle should be close to zero; we can have confidence in the location if the angle is below ≈15°.

The reactance method divided the reactive portion of the measured impedance by the reactive portion of the line impedance; there was no resultant angle, only magnitude. Using the fault data, we generated a graph that showed each variable's effect on fault location. Using the calibration results, we were then able to derive a delta value for the change in fault location, which allowed us to form a range of calibration error for each fault.

III. Implementation

We used a function in our analysis software to extract fault values one cycle after the fault recorder trigger time. We then wrote a program using Octave [1] (an open-source MATLAB-compatible program) to read the data, perform fault location, adjust the calibration by either ±10% or ±10°, and then output the calculations, graphs, and fault location deltas.

To extract the data from the DFR and relay records, we created a template for our analysis tool that told the program which data to extract from the fault files. The software opened one file at a time, processed each line group, then wrote the fault data to a *.csv* file. The data included the magnitude and angle of each voltage and current measurement, as well as the parameters associated with each line. The template allowed us to process multiple files automatically, which allowed us to quickly build a file with all of our selected faults.

Since the *.csv* file contained all the faults extracted, we only needed to manually remove the line groups that were not part of our area of study. We used the varied data along with input data in the fault location calculations for each voltage, current, and line parameter. A graph was created for each varied input parameter and showed the results of the simulated calibration's fault locations.

IV. Fault Selection

To get a diverse set of data for these tests, we selected faults from all of our transmission voltage levels, all different fault types (phase-to-ground, phase-to-phase, and three-phase), as well as lines of different lengths. We decided to sample a few outlier faults to see if, for example, low fault current or highly resistive faults showed any significant differences in the calibrated fault locations. Most of the faults we studied were phase-to-ground faults, which is the most common type on our transmission system. Table II identifies each of the 32 faults we sampled by fault type and voltage level.

Table II
Number of Faults Per Fault Type

P-G			**P-P**			**3P**	
A-G	B-G	C-G	A-B	B-C	C-A	A-B-C	Total
10	6	8	4	1	1	2	32

To see if the length of the line bore any significance on fault location, we chose faults with a wide range of line lengths. The shortest line sampled was 2.86 miles long, and the longest line was 77.65 miles long.

V. Fault Data

Fault data was obtained for each of the 32 faults selected. This section of the paper highlights the fault data for just one of the faults we studied.

This case was a C-G phase-to-ground fault on a 230 kV transmission line that is 44.39 miles long. The result of varying the current by ±10% is shown in Fig. 1 (found in Appendix A.)

The top graph shows the magnitude results of the two fault location calculations—simple and reactance. These methods are described in [2]. The bottom graph shows the change in the fault location's resultant angle when using the simple method. The simple method uses complex numbers, so the results include both a magnitude and an angle.

We were primarily interested in the graphs and deltas that correlated with the variations in faulted phase input values. The script created similar graphs for all the variations; since this was a C-G fault, variations in A and B-phase voltages and currents had no effect on the fault location calculation and were excluded. In addition to the graphs, the script outputs a .txt file that shows the deltas for every varied input in miles. These deltas

are calculated by taking the absolute value of the fault location calculated at +10% calibration subtracted by the fault location calculated at -10% calibration. An example of the C-phase currents from the output fault location deltas report can be seen in Table III.

Table III
Output Fault Location Deltas

Calculation Method	Delta (miles)
Ic_Mag Fault Location Mag Delta	2.9983
Ic_Mag Fault Location Reactance Delta	3.0612
Ic_Mag Fault Location Ang Delta	0.8322

In this case, the change in fault location was mostly linear. As shown in Table III, the ±10% variation in current resulted in about a ±1.5 mile variation in fault location. The change in resultant angle was very small. The ±1.5 mile variation equates to about a ±3.3% change in fault location. However, since this is a relatively long line, 3.3% can be a significant error.

Fig. 2 graphs the fault location trend when the C-phase voltage was varied by ±10%. The delta in the fault location was slightly greater than 5 miles, ±2.6 miles. For a 44.39-mile-long line, the ±10% change in voltage resulted in a ±5.8% change in fault location seen on the line length. (See Fig. 2 in Appendix A.)

VI. Results

We analyzed and summarized the data according to the type of fault—phase-to-ground, phase-to-phase, or three-phase—to determine if there were any common patterns.

A. Phase-to-ground faults

The spread of phase-to-ground faults is included in Table II. A few were outliers and will be discussed later in this section.

In total, 24 phase-to-ground faults were analyzed, and we discovered a few key insights that helped us understand the effect that calibration can have on fault location. The only input quantities that showed any change on fault location in A-phase-to-ground faults were the quantities associated with the faulted phase. For example, when the B and C-phase voltages and currents were varied for an A-G fault, no change was observed in the calculated fault location. This is exactly the behavior we would expect. The input values that were affected in an A-G fault were A-phase voltage, A-phase current, residual current, and all of the line characteristics.

Most of the trends were linear for the varied magnitude values of the affected input phasors. The voltage-varied fault location trends directly correlated to the increasing voltage throughout the ±10% variance (see Fig. 2). The current-varied fault location trends were inversely correlated to the increasing current (see Fig. 1). This pattern can be observed in all phase-to-ground fault cases regardless of the fault impedance.

B. Phase-to-phase faults

Fault location trends showed a few minor differences in phase-to-phase faults. Due to the nature of the fault, when the residual current was varied, there was no longer any effect on the fault. We also noticed that when the line's zero-sequence impedance was varied, the fault location showed no changes. For example, in one of the cases we studied, an A-phase-to-B-phase fault showed that the fault location trends directly correlated to the varied voltage magnitude for both of the faulted voltages. The fault location for the currents was inversely correlated. (See Fig. 3 in Appendix A.)

The correlations seen in the P-G and P-P faults were due to the fault impedance (Z_f) derived from the formulas for the simple and reactive fault location methods. In the formula for Z_f, the voltage vector is divided by the current vector to calculate the fault impedance, which becomes the numerator in the following calculations to get the fault location vector. And so, when the voltage increased as everything else remained constant, the fault location magnitude directly correlated to that linear increase. The same rules applied to currents. When the current was increased, the fault location magnitudes decreased.

C. Three-phase faults

Our 32-fault sample only had two three-phase faults, and they behaved similarly. As one may expect, the three faulted phases were affected by variations in both voltage and current; but the residual or ground current showed no delta in fault location.

A three-phase fault, by its nature, can be considered a phase-to-phase fault, and it shares most of its properties. We used the same fault calculation methods as phase-to-phase, but we used positive sequence voltage and positive sequence current to calculate Z_f. Therefore, the three-phase graph trends look very similar to the phase-to-phase graphs.

D. Outliers

We included outliers in our fault samples to see if they would perform similarly to the more common cases. The most prominent outlier was a high-impedance fault due a broken conductor on the ground, which caused very low fault current. The voltage rating on the line was 115 kV and the fault current at the time of the sample was 890 amps. The line is roughly 10 miles long, and the delta fault location was calculated to be 7.8 miles, or 77.57% of the line length.

Another outlier with a low fault current was included in the sample to determine if these two outliers would behave the same. The second outlier did not have as dramatic a range of fault locations, as its line properties were different. In the second case the line was a little over 43 miles long and the fault had a large zero sequence contribution at the time, which was sourcing from somewhere else in the system. Those two factors alone could explain why we did not see similar behavior in these faults.

Additionally, there was a fair mixture of higher-impedance faults inserted into the fault samples, these were found to be resistive faults in nature caused by vegetation or contamination. The deltas in fault locations for the sample size of these faults were not consistently significant enough to be highlighted in the conclusion of this paper.

VII. Results Table

Table IV (see in Appendix B) includes the data gathered from all 32 faults. The variations in fault locations are grouped into three areas of interest: the length of the line, the voltage rating of the line, and the fault type experienced. This data is a combination of averages and median values, expressed in miles, taken from the calculated fault location deltas and the percents calculated by the Octave program.

We decided to display the median values as a check for the outliers that are present in the faults sample. The values representing average delta are in bold and median values are not in bold.

VIII. Conclusions

Each line has defined impedance properties, and the system conditions can vary at any point in time; it becomes difficult to be certain that the similarities we saw across the 32 unique faults are constant and can translate to other parts of the power grid. However, the results we gathered from the output data allowed us to draw a few conclusions.

The data show that variations in fault voltage have a more pronounced effect on the fault location deltas than variations in fault currents.

For extreme line lengths—shorter than 4 miles and longer than 35 miles—a larger percent of the line fault location delta was experienced when the fault phase values were varied. For example, on the longest line sampled (77.65 miles) the delta for fault location was calculated to be >2.0 miles for just about every varied input. However, when we calculated the error using the percent of the line length, the delta was only ~2.5%—a much more reasonable number when taking the lines length into account..

This calculation method confirms that when input values are calibrated on a longer line, the fault location delta in miles is going to be larger, on average, than on the smaller lines. But from the perspective of total line length, that delta may not be significant. A similar pattern occurs in shorter lines: the percent of the fault location delta is much greater than the percents seen for medium-to-long lines. For example, a 0.5-mile-long fault location delta for a three-mile-long line is 16.6% of the line, whereas that same 0.5-mile delta is only 2.5% of a 20-mile-long line. To reiterate, short lines experience more change in fault location delta measured as percent of line length, but the long lines show more change in fault location delta independent of the physical line length. Therefore, from a restoration perspective, long lines are more sensitive to calibration errors.

In summary, the calibration of the input variables used to calculate fault location in a DFR does matter; however, it may not matter as much in some cases.

In this case study we varied the input values from ±10% which is much greater than the acceptable range of ±0.5% we use in our calibration procedure. So, in respect to what we declare as acceptable the 90-110 V variation from an input of 100 V is exaggerated. Even with such a wide range, we still had calculated fault locations that were within a mile of the actual location, suggesting that in these cases calibration is not needed.

For the cases where we observed a significant effect on fault location with a calibration range of ±10%, when we compare that to a realistic calibration range of ±0.5%, or even ±2%, our results are not nearly as exaggerated and are acceptable.

Assuming that the fault location trend is linear, and in almost every case it is, we can accurately down-sample our study to observe changes in fault location over a range of ±0.5% by dividing the delta from our ±10% range by 20. This showed us that in our worst-case, the first outlier, the delta was only 0.39 miles, instead of 7.8 miles. For a well-behaved sample, we see a delta of 0.0066 miles instead of 0.13 miles. For the purposes of the study a ±10% shows the extent of what could occur due to loss of calibration or miscalibration. The results in Table IV (see in Appendix B) show that even under the extremes, the average delta of all of the samples in each category is no greater than two miles on either end of the actual fault location.

Over the years, Dominion Energy's expectations for fault location accuracy have changed considerably. In the late 1990s, any fault location that was ±2 miles was considered good. Now that we have multiple fault location methods, better monitoring coverage, and automated systems, we expect to be able to pinpoint fault locations within half a mile. The results of this study reveal the extent of the affects that DFR calibration have on fault location and based on these results, our current DFR calibration specifications meet our needs for accurate fault locating.

References

[1] John W. Eaton, David Bateman, Søren Hauberg, Rik Wehbring (2022). GNU Octave version 7.3.0 manual: a high-level interactive language for numerical computations. URL https://www.gnu.org/software/octave/doc/v7.3.0/

[2] IEEE Guide for Determining Fault Location on AC Transmission and Distribution Lines, IEEE Standard C37.114-2014, 2014

Biographies

Ethan M. Mueller has worked at Dominion Energy in the System Protection Automation and Analysis group since 2022. His main responsibilities are post event analysis, event reporting, and database maintenance for fault events on the system. He received a bachelor's degree in electrical engineering from Old Dominion University in 2022.

Robert M. Orndorff has been at Dominion Energy since 1984. He spent 11 years as a field relay technician and moved to the Fault Analysis department in 1997 where he still works. His interests include fault location, grid frequency events, and analyzing unusual operations. Robert graduated from J Sargeant Reynolds Community College in 1986 with an AAS degree in

Electricity and Electronics. He is a member of IEEE and has been a member of the TRUC planning committee since 2003.

Micah J. Till is the manager of System Protection Engineering. His work history includes Dominion Energy's supervisor of Electrical Transmission System Protection Automation & Analysis at Dominion Energy, Special Studies, Reliability Engineering, System Protection Engineering, Electric Transmission Planning, and Operations Engineering groups. He has also worked at Tennessee Valley Authority in Chattanooga and ABB Group in Baden, Switzerland. He received his PhD from the University of Tennessee, Knoxville in 2017.

Amir Makki has worked at Softstuf since 1991. His main interest is automating fault and disturbance data analysis. He is extensively published and holds a number of U.S. patents and trademarks. Amir is a senior member of IEEE and is an active member of the Protection Systems Relay Committee where he chaired several working groups including COMTRADE, COMNAME, and the Cyber Security Task Force for Protection Related Data Files. He has BS and MS degrees in Electrical Engineering from Tennessee Tech University and pursued his Ph.D. studies in Software Engineering at Temple University.

Maria Rothweiler has worked at Softstuf since 1991. Her main interest is developing software tools to display and analyze power system fault and disturbance data. She is extensively published and holds a number of U.S. patents, trademarks, and copyrights. Maria is a member of IEEE and an active member of the IEEE Standards Association. She holds a Bachelor of Arts degree in Computer Science from Temple University and pursued her associate degree in mathematics at Bucks County Community College.

APPENDIX A

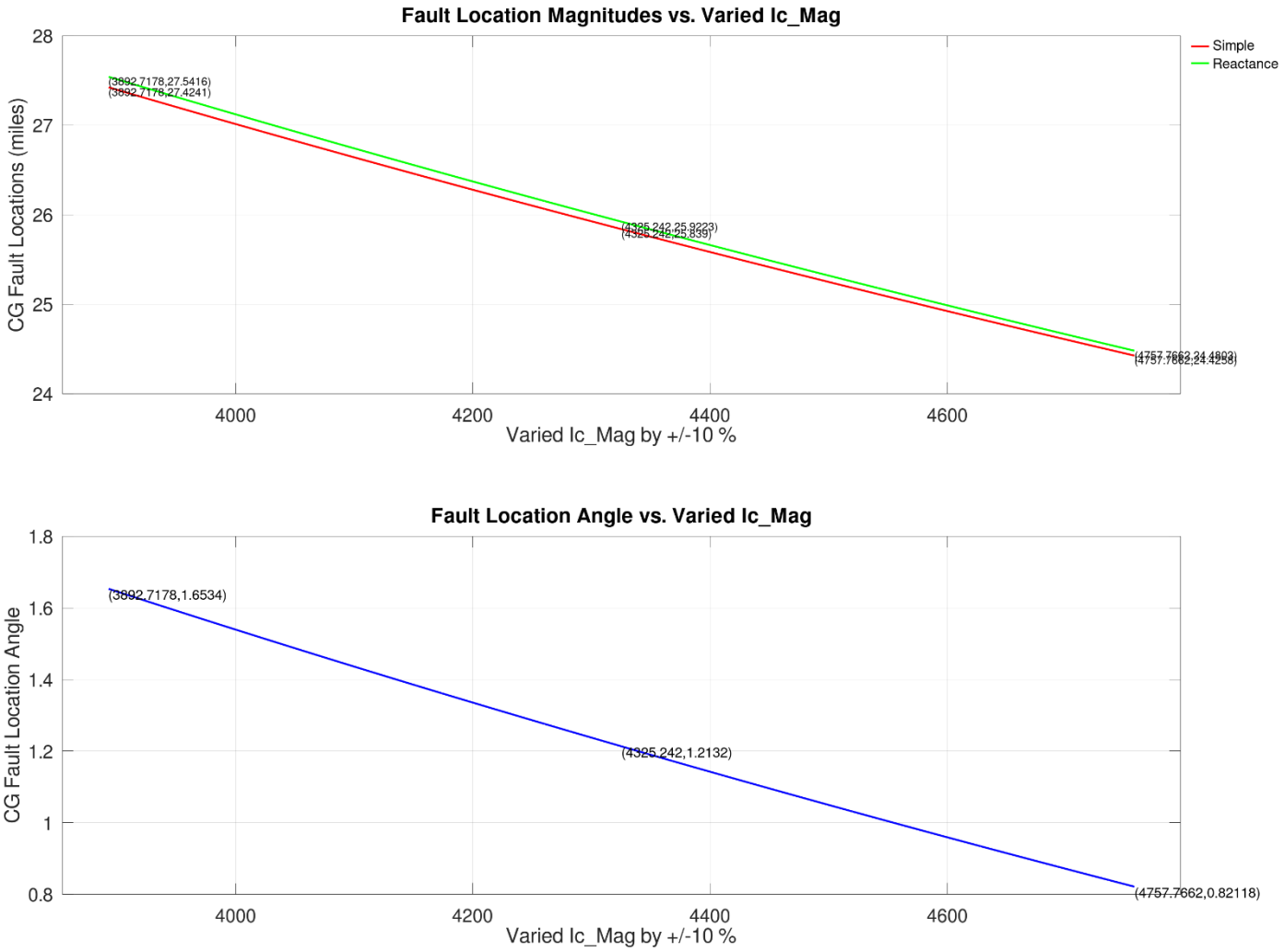

Fig. 1. Example of A-phase-to-ground varied current

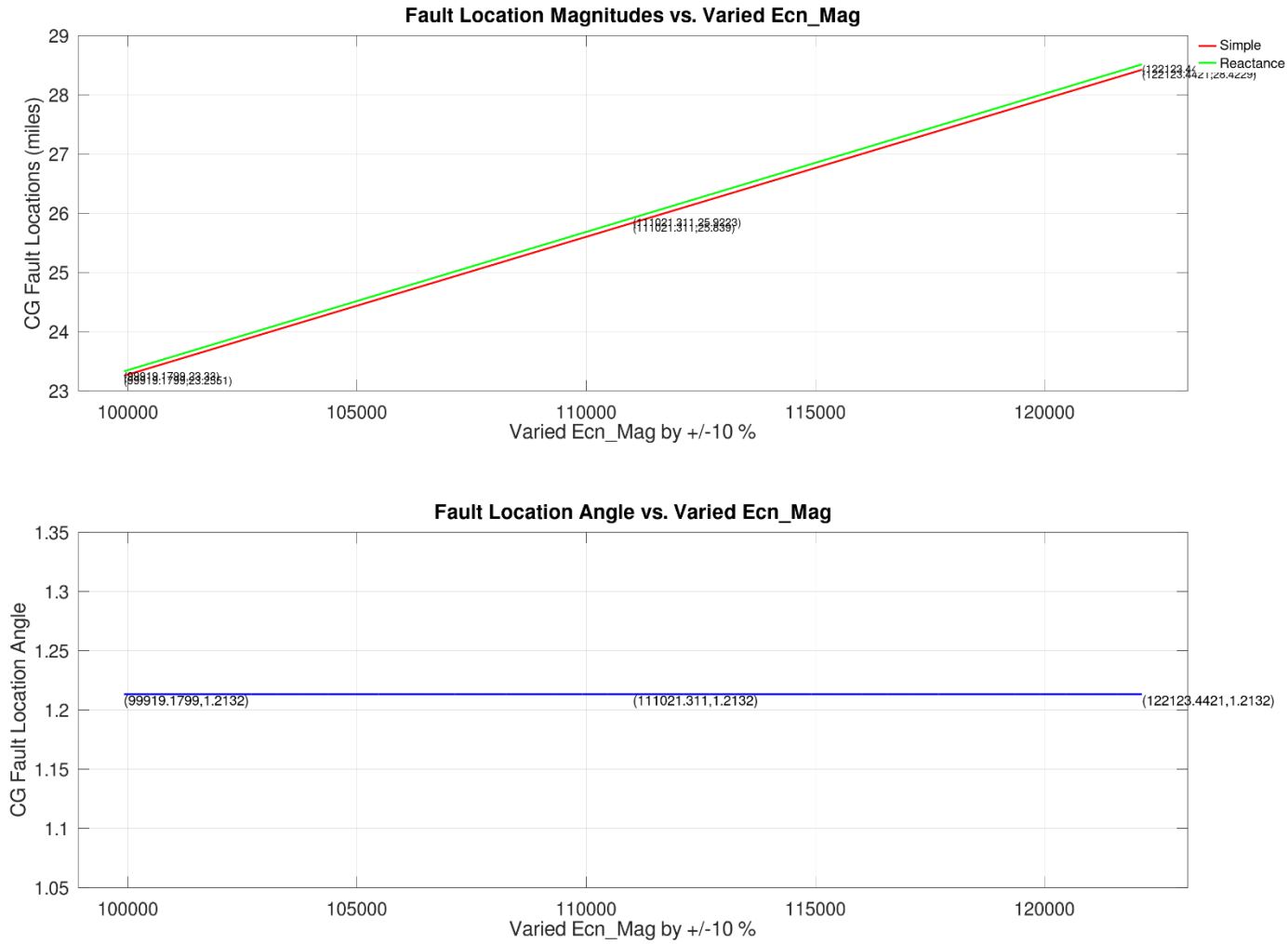

Fig. 2. Example of phase-to-ground varied voltage

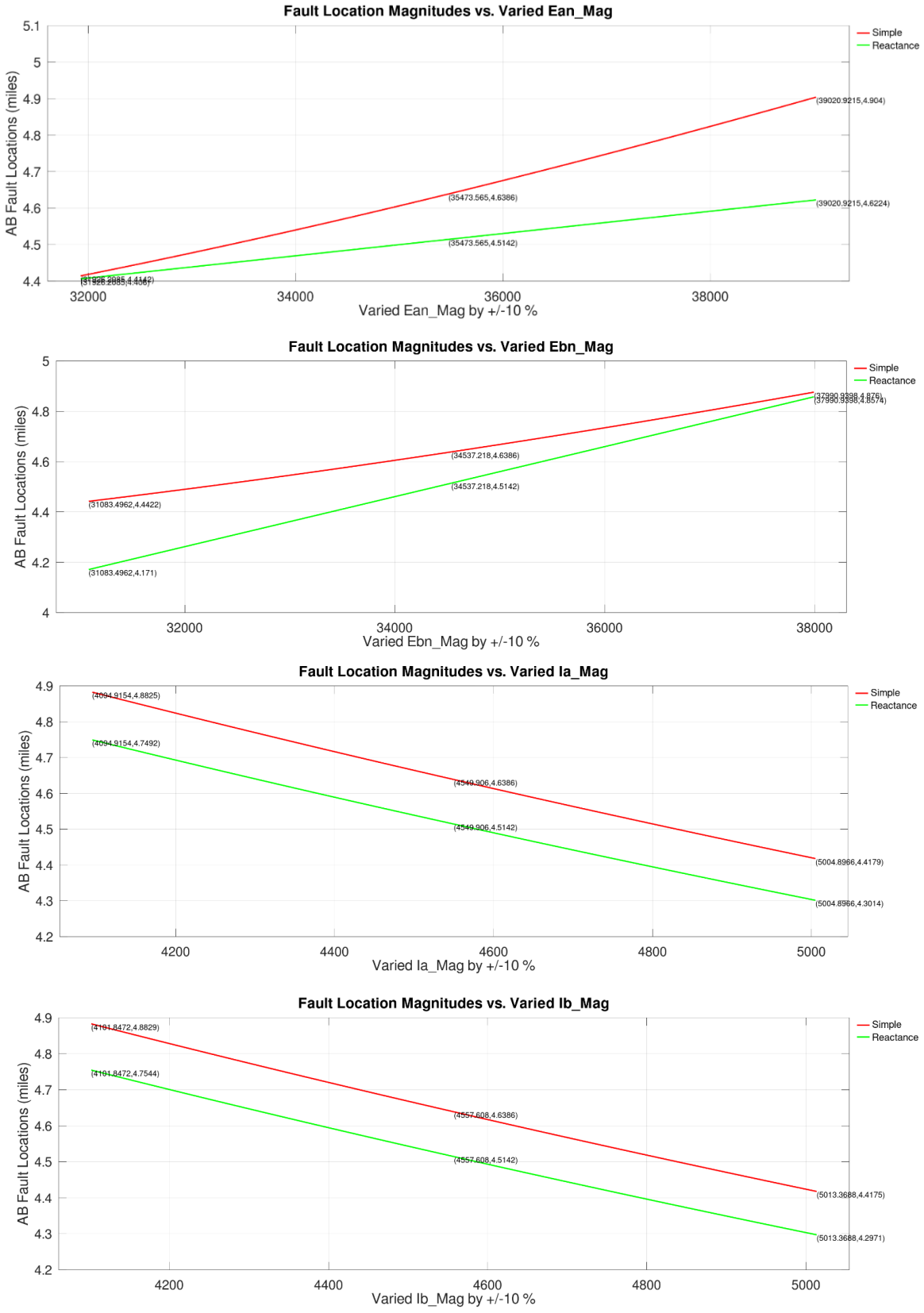

Fig. 3. Phase-to-phase varied inputs.

APPENDIX B

Table IV
Fault Location Variations

Fault Location Variations																
Line/fault type	**# of Faults**	**Calc Method**	**Current ± 10%**				**Voltage ± 10%**				**Angle ± 10%**					
			Simple (miles / %)		**Reactance (miles / %)**		**Simple (miles / %)**		**Reactance (miles / %)**		**Simple (miles / %)**		**Reactance (miles / %)**			
Long lines	**6**	**Average**	**2.1969**	**5.16%**	**2.0976**	**4.91%**	**3.7192**	**9.02%**	**3.4081**	**8.24%**	**0.5074**	**0.84%**	**1.7482**	**4.09%**		
		Median	2.2308	5.62%	2.1932	4.95%	3.6796	10.33%	3.1026	8.83%	0.1473	0.42%	1.6213	2.89%		
Medium lines	**12**	**Average**	**1.0433**	**5.59%**	**0.9000**	**4.99%**	**1.6073**	**8.55%**	**1.3734**	**7.48%**	**0.1181**	**0.80%**	**1.0804**	**5.53%**		
		Median	0.6583	3.63%	0.6317	3.20%	1.1459	6.11%	1.0520	5.41%	0.0584	0.21%	0.7522	3.40%		
Short lines	**14**	**Average**	**0.6410**	**8.82%**	**0.3802**	**6.10%**	**0.9831**	**13.13%**	**0.5095**	**8.19%**	**0.2150**	**3.38%**	**1.2032**	**14.64%**		
		Median	0.2772	4.87%	0.2273	4.71%	0.4250	6.39%	0.3405	5.50%	0.0296	0.49%	0.3496	6.03%		
115kV lines	**14**	**Average**	**1.0702**	**8.75%**	**0.7080**	**5.71%**	**1.6692**	**13.36%**	**1.0582**	**8.06%**	**0.1044**	**1.65%**	**1.6332**	**13.98%**		
		Median	0.4258	5.38%	0.4169	5.12%	0.6230	6.85%	0.5646	5.77%	0.0228	0.20%	0.5349	5.94%		
230kV lines	**14**	**Average**	**0.8025**	**5.40%**	**0.7792**	**5.20%**	**1.3457**	**8.26%**	**1.2480**	**7.54%**	**0.2420**	**2.45%**	**0.7534**	**6.05%**		
		Median	0.4968	3.63%	0.4691	3.39%	0.8829	6.43%	0.8188	5.95%	0.1093	0.52%	0.7022	4.00%		
500kV lines	**4**	**Average**	**2.1138**	**5.83%**	**1.9725**	**5.51%**	**3.2983**	**9.55%**	**2.9267**	**8.63%**	**0.6554**	**1.13%**	**1.7212**	**3.85%**		
		Median	2.0902	5.63%	1.9990	4.95%	3.2023	10.33%	2.4890	8.57%	0.1721	0.71%	1.4325	2.34%		
P-G	**24**	**Average**	**1.5549**	**8.35%**	**1.0010**	**5.53%**	**2.0955**	**12.25%**	**1.6334**	**8.74%**	**0.0848**	**0.48%**	**1.4033**	**9.50%**		
		Median	0.6583	5.56%	0.6406	3.97%	1.1459	8.19%	1.0520	6.60%	0.0512	0.32%	0.6241	4.26%		
P-P	**6**	**Average**	**0.7183**	**5.43%**	**0.7047**	**5.30%**	**0.7662**	**5.98%**	**0.7345**	**5.64%**	**0.9003**	**8.25%**	**1.0535**	**10.20%**		
		Median	0.4560	3.23%	0.4320	3.08%	0.4530	3.79%	0.4309	3.08%	0.7364	6.16%	0.9044	10.11%		
3-P	**2**	**Average**	**0.2389**	**5.38%**	**0.2273**	**5.12%**	**0.2387**	**5.37%**	**0.2270**	**5.11%**	**0.0174**	**0.40%**	**0.1492**	**3.35%**		
		Median	0.2389	5.38%	0.2273	5.12%	0.2387	5.37%	0.2270	5.11%	0.0174	0.40%	0.1492	3.35%		